SKIN

Cell and fluid sampling microneedle patches for monitoring skin-resident immunity

Anasuya Mandal[1,2,3], Archana V. Boopathy[2], Lionel K. W. Lam[1,2], Kelly D. Moynihan[2,4], Mary E. Welch[2], Nitasha R. Bennett[2], Michelle E. Turvey[5], Nikki Thai[2], Jenny H. Van[4], J. Christopher Love[1,2,3,6], Paula T. Hammond[1,2,3,5]*, Darrell J. Irvine[2,3,4,6,7,8]*

Important cell populations reside within tissues and are not accessed by traditional blood draws used to monitor the immune system. To address this issue at an essential barrier tissue, the skin, we created a microneedle-based technology for longitudinal sampling of cells and interstitial fluid, enabling minimally invasive parallel monitoring of immune responses. Solid microneedle projections were coated by a cross-linked biocompatible polymer, which swells upon skin insertion, forming a porous matrix for local leukocyte infiltration. By embedding molecular adjuvants and specific antigens encapsulated in nanocapsules within the hydrogel coating, antigen-specific lymphocytes can be enriched in the recovered cell population, allowing for subsequent detailed phenotypic and functional analysis. We demonstrate this approach in mice immunized with a model protein antigen or infected in the skin with vaccinia virus. After vaccination or infection, sampling microneedles allowed tissue-resident memory T cells (T_{RM}s) to be longitudinally monitored in the skin for many months, during which time the antigen-specific T cell population in systemic circulation contracted to low or undetectable counts. Sampling microneedles did not change the immune status of naïve or antigen-exposed animals. We also validated the ability of cell sampling using human skin samples. This approach may be useful in vaccines and immunotherapies to temporally query T_{RM} populations or as a diagnostic platform to sample for biomarkers in chronic inflammatory and autoimmune disorders, allowing information previously accessible only via invasive biopsies to be obtained in a minimally invasive manner from the skin or other mucosal tissues.

INTRODUCTION

Current methods for accessing compartments of the body to obtain samples of tissues, cells, or fluid for medical diagnosis and monitoring fall into three categories: (i) invasive, such as via traditional phlebotomy; (ii) minimally invasive, such as saliva swabs; and (iii) noninvasive, such as urine collection. Immune monitoring is performed primarily by analysis of blood draws, a practice in use since the early times (*1*), with analysis by flow cytometry of peripherally sampled blood as the most prevalent method for immunophenotyping (*2*, *3*). However, many important immune cell populations preferentially reside in peripheral tissues including barrier tissues such as the skin, gut, and other mucosal surfaces and do not recirculate in the blood. This includes tissue-resident macrophages, natural killer (NK) cells, NK T cells, B cells, plasma cells, and memory T cells (*4*–*6*). Notably, a larger proportion of T cells reside in peripheral tissues than in the secondary lymphoid organs at steady state (*7*). Resident memory T cells (T_{RM}s) reside in the skin and other mucosal tissues without recirculation in the blood (*8*) and include cytotoxic $CD8^+$ T cells poised for immediate interception and killing of infected cells, providing a critical frontline response to infection (*9*). These cells are not accessed by traditional blood-based analysis of the immune response.

Current approaches for monitoring tissue-resident immune cell populations are limited. One widely used method to query the skin is via delayed type hypersensitivity tests such as the Mantoux test (*10*) and allergen patch tests (*11*, *12*), which offer qualitative readouts of an immune response toward a particular antigen. In the case of the tuberculin Mantoux test, the tuberculin antigen is injected into the dermis, and the skin is monitored for the next 2 to 3 days for the development of an induration, which indicates the presence of a recall immune response. However, these methods fail to offer quantitative information about phenotypic and functional aspects of the cell infiltrate. There exist invasive methods of sampling immune cell populations from lymph nodes (*13*) or from skin (*14*), but these are apparatus intensive and require special training for use. Minimally invasive methods for quantitative monitoring of the immune status of the skin or other barrier tissues could provide valuable information in the context of patients with genetic and acquired immunodeficiency disorders, organ transplants, and vaccination, but such approaches are currently lacking.

Microneedle patches, arrays of typically submillimeter pyramidal or conical projections designed to mechanically pierce the stratum corneum and reach the viable epidermis/upper dermis, have been extensively explored for delivery of drugs and vaccines into the skin (*15*). However, a variety of microneedles have also been designed to extract interstitial fluid (ISF) from the skin, enabling monitoring of glucose, antibodies, or other biomarkers, including solid microneedles, to simply perforate the skin and enable access to ISF (*16*). Although these are effective minimally invasive technologies, to date, only sampling of soluble biomolecules has been demonstrated.

Here, we demonstrate a microneedle-based platform for the combined sampling of ISF and viable cells from the skin. Using solid microneedles coated by a sampling hydrogel layer that swells on application to the skin, we demonstrate recovery of leukocytes that infiltrate the sampling layer. Mimicking the classical Mantoux test, we further show that, by incorporation of antigen- and adjuvant-carrying

[1]Department of Chemical Engineering, MIT, Cambridge, MA 02139, USA. [2]Koch Institute for Integrative Cancer Research, MIT, Cambridge, MA 02139, USA. [3]Institute for Soldier Nanotechnologies, MIT, Cambridge, MA 02139, USA. [4]Department of Biological Engineering, MIT, Cambridge, MA 02139, USA. [5]Infectious Diseases IRG, Singapore-MIT Alliance for Research and Technology, Singapore 138602, Singapore. [6]Ragon Institute of MGH, MIT and Harvard, Cambridge, MA 02139, USA. [7]Department of Materials Science and Engineering, MIT, Cambridge, MA 02139, USA. [8]Howard Hughes Medical Institute, Chevy Chase, MD 20815, USA.
*Corresponding author. Email: hammond@mit.edu (P.T.H.); djirvine@mit.edu (D.J.I.)

nanoparticles into the sampling layer, forming stimulatory sampling microneedles (SSMNs), we can specifically enrich for antigen-specific T_{RM}s and memory cells, without perturbing the immune status of animals. This technology thus provides an innovative means for minimally invasive monitoring of key immune cell populations of interest in vaccination, infectious disease, and autoimmune disorders.

RESULTS

Alginate-coated microneedles can be fabricated to sample cells and ISF

The conceptual design that we pursued is outlined in Fig. 1A: A skin patch composed of a square array of pyramidal solid polymer microneedles (each 250 μm in width at the base and ~600 μm in height) is coated with a biocompatible hydrogel layer. Embedded within the gel layer are adjuvants and lipid nanocapsules containing an antigen of interest [Fig. 1A (a)]. Upon application to the skin, the hydrogel layer swells with the intake of ISF [Fig. 1A (b)]. Antigen-presenting cells (APCs) migrate into the alginate matrix in response to the localized inflammation induced by microneedle penetration into the skin (*17*), are activated by the adjuvant, and take up the embedded antigen-carrying nanocapsules [Fig. 1A (c)]. Cytokines and chemokines produced by these activated APCs in turn promote recruitment of T cells into the gel coating. T cells specific for antigen presented by the nanocapsule-loaded APCs will be retained in the gel layer, enriching these antigen-specific cells. Upon removal of the microneedles from the skin, the hydrogel layer is dissolved, releasing cells for analysis by diverse immunological tools for phenotyping and immune profiling [Fig. 1A (d and e)]. We hypothesized that such a design would simultaneously allow ISF to be sampled and provide a window into the antigen-specific immune cell populations in the skin.

To implement this design, polymer microneedle arrays were formed by melt-molding polylactide (*18*), and alginate was selected as a biocompatible hydrogel coating material (*19*). To select an alginate composition, we compared cellular infiltration into subcutaneously implanted alginate gels composed of low or high molecular weight ("Lo MW," 75 kDa; "Hi MW," 200,000 kDa) and with different alginate concentrations. Basal cellular infiltration into alginate matrices was similar in Lo MW and Hi MW gels composed of 1 weight % (wt %) alginate, which had an elastic modulus of ~1 kPa, ensuring sufficient mechanical stiffness (fig. S1, A and B). Hi MW alginate was chosen for better mechanical integrity and ease of handling. Microneedles were first coated with an absorbed layer of polylysine to promote electrostatic adhesion of the alginate to the underlying microneedle surface, followed by drop casting of an alginate/sucrose solution, cross-linking of the alginate coating by application of calcium chloride, and drying to a solid alginate/sucrose layer (Fig. 1B). Interbilayer–cross-linked multilamellar vesicles (ICMVs) (*20*), lipid nanocapsules (diameter, ~125 nm) carrying antigen and adjuvant (described further below), were added to the alginate solution before drop casting to incorporate these components into the alginate matrix. Sucrose was included in the gel layer to increase the mechanical integrity of the alginate coating during initial penetration of the stratum corneum and to act as an in situ porogen, increasing the porosity of the alginate as it swells in the skin. Trypan blue staining confirmed that alginate/sucrose-coated microneedles efficiently penetrated the skin of mice (Fig. 1C). Microneedles exposed to PBS for 20 min showed rapid rehydration and swelling of the alginate layer by ~3-fold in thickness from its dried state (Fig. 1, D to F). In addition, we evaluated the potential for ISF sampling with the gel layer. In vitro, microneedles exposed to solutions of immunoglobulin G (IgG) or IgM and then digested for analysis of protein content by enzyme-linked immunosorbent assay (ELISA) gave accurate measurements of the bulk solution concentration of IgG or IgM solutions (fig. S2).

Sampling microneedles can be used for the recovery of cells and ISF

We were particularly interested in sampling of antigen-specific skin T_{RM}s, and thus, we first established a model immunization protocol to generate a defined population of skin-resident T_{RM}. Mice were vaccinated twice subcutaneously at the base of the tail, with ovalbumin (OVA) protein and lipid-conjugated CpG, a Toll-like receptor 9 (TLR9) agonist. Four weeks later, cell suspensions from blood and digested ear tissue were stained with carboxyfluorescein diacetate succinimidyl ester (CFSE) to distinguish cells from tissue digest debris, and OVA-specific $CD8^+$ T cells expressing T_{RM} markers were identified by flow cytometry (fig. S3A). We defined these cells conservatively as $CD69^+CD103^+$ T cells, although it is known that T_{RM} may lack expression of one or both of these markers in some tissues (*7*). High numbers of OVA-specific $CD8^+$ T cells were detected in the blood at this time point (fig. S3, B and C), and ear tissue showed the presence of antigen-specific $CD69^+CD103^+$ T_{RM}s (fig. S3, B to D).

To evaluate the potential of alginate-coated microneedles to sample tissue-resident cells and ISF, we next modeled a classic delayed type hypersensitivity/Mantoux test (Fig. 2A). Naïve or OVA-immunized mice were injected intradermally in the ear with OVA and adjuvant. Five days later, alginate-coated microneedles containing no antigen or adjuvants in the gel coating were applied for 12 hours to the same skin site and then retrieved for analysis. To retrieve sampled cells, the alginate layer was dissolved in the presence of EDTA, and recovered cells were stained with antibodies, labeled with CFSE to aid in distinguishing live cells from alginate debris, and analyzed by flow cytometry (Fig. 2B). As shown in Fig. 2 (C and D), naïve mice showed no detectable OVA-specific $CD8^+$ T cells in the blood, whereas OVA-specific T cells were present at high numbers in immunized mice even at 4 weeks after vaccination. Sampling microneedles also recovered a substantial $tetramer^+$ population at the site of the antigen injection from immunized animals, although with lower total numbers of cells collected compared to the blood sample (Fig. 2, C and D). We then compared OVA-specific IgG titers by ELISA on ISF recovered from the same microneedle patches versus serum samples from the same animals. Consistent with previous studies comparing serum and ISF (*21*, *22*), OVA-specific IgG was easily detected in microneedle-recovered ISF from immunized mice, at a lower titer than serum from the same animals (Fig. 2E).

Adjuvant incorporation increases cell recovery by sampling microneedles

To simplify from the two-step sampling strategy performed in the experiments of Fig. 2, we next investigated whether a one-time application of microneedles loaded with molecular adjuvants would lead to effective cell recovery. On the basis of the expression of TLRs in keratinocytes and skin-derived dendritic cells, we tested the TLR3 agonist polyI:C and TLR1/2 agonist pam3Cys (*23*, *24*). Intradermal injection of pam3Cys led to recruitment of $CD8^+$ T cells and myeloid cells into the skin of C57Bl/6 mice, which was substantially augmented by coadministration of polyI:C (fig. S4, A and B). Inclusion of this adjuvant combination in alginate hydrogels implanted subcutaneously

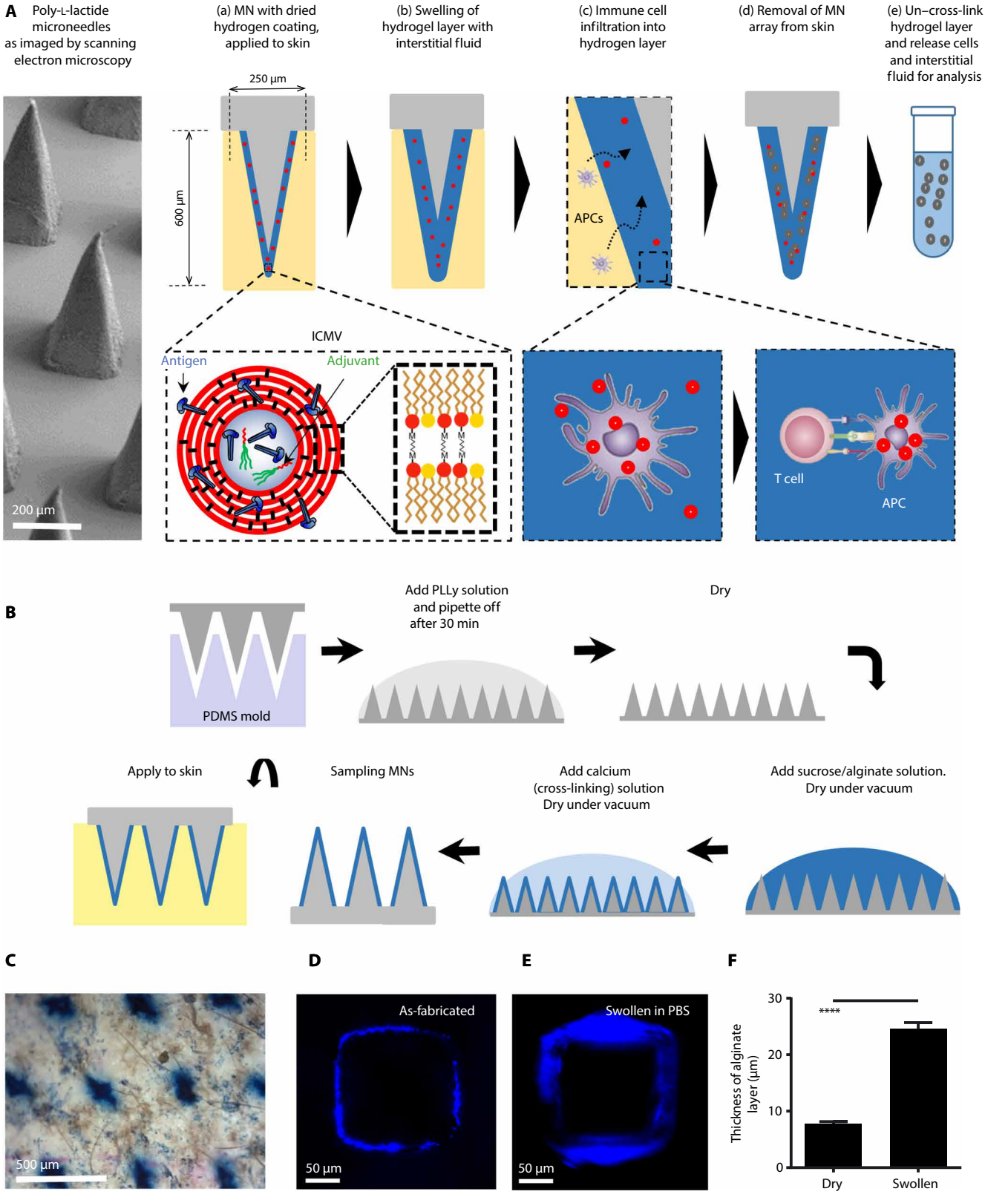

Fig. 1. Fabrication of SSMNs platform for immune monitoring. (**A**) Schematic of SSMN structure and proposed mechanisms of action. (**B**) Microneedle (MN) fabrication process. PLLy, poly-L-lysine; PDMS, polydimethylsiloxane. (**C**) Trypan blue stain of mouse ear tissue. (**D** to **F**) Confocal micrographs showing a cross section of the alginate layer (blue) on an individual microneedle projection before (D) and after (E) swelling in phosphate-buffered saline (PBS) for 20 min at 25°C. (F) Thickness of alginate layer quantified before and after PBS swelling. ****$P < 0.0001$, analyzed by two-tailed nonparametric Mann-Whitney test.

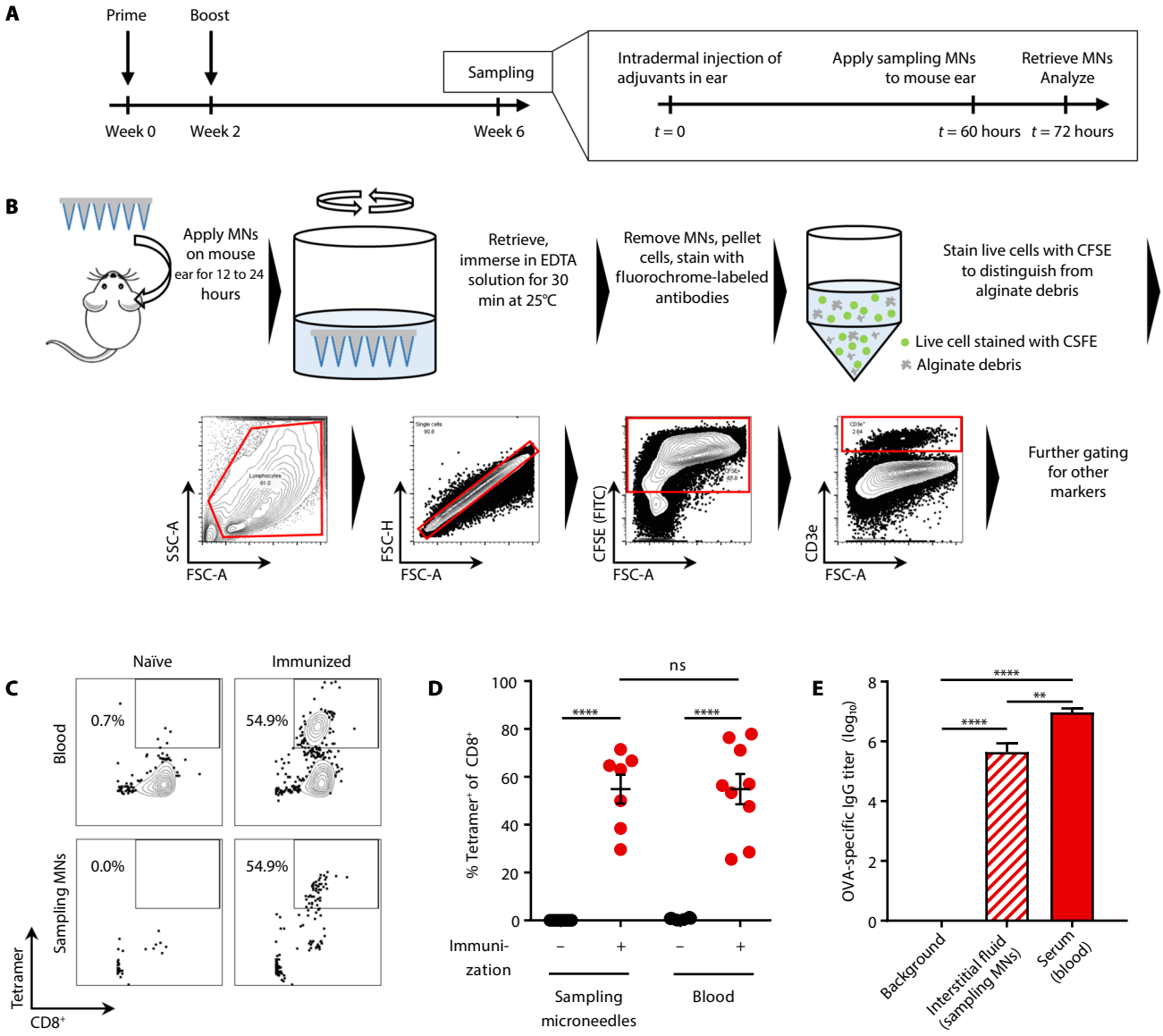

Fig. 2. Cell sampling microneedles allow tandem analysis of cellular and humoral immune responses. (**A**) Groups of OVA-immunized or naïve C57Bl/6 mice ($n = 9$ per group) were injected intradermally in the ear at time zero with 2 μg of OVA and 5 μg each of adjuvants polyI:C and pam3Cys. Sixty hours later, sampling microneedles were applied to the same site for 12 hours, followed by retrieval and flow cytometry analysis. (**B**) Sample processing and flow cytometry gating strategy. FITC, fluorescein isothiocyanate. (**C** and **D**) Representative flow cytometry plots (**C**) and quantification from groups of animals (D) showing OVA-specific SIINFEKL/H-2K^b–streptavidin tetramer$^+$CD8$^+$ T cells, as sampled from blood or with cell sampling microneedles. (**E**) OVA-specific IgG titers ($\log_{10}$) as quantified from serum or ISF from sampling microneedles. Data shown are means ± SEM from one representative of two independent experiments. ns, nonsignificant, $^{**}P < 0.01$, $^{****}P < 0.0001$, analyzed by one-way analysis of variance (ANOVA), followed by Tukey's honestly significant difference (HSD).

in enhanced green fluorescent protein (eGFP) mice (expressing GFP in all nucleated cells) also resulted in significantly higher ($P < 0.05$) cell infiltration into the gel compared with alginate alone (fig. S4, C and D).

PolyI:C is high molecular weight double-stranded RNA, which we expected to be retained effectively in the microneedle alginate coating, but pam3Cys is a small lipopeptide that may not be retained because of rapid diffusion from the gel layer. To promote retention of the latter and codelivery of adjuvant signals with incorporated antigen to infiltrating APCs, we prepared pam3cys-loaded ICMV lipid capsules (mean diameter of 126 ± 11 nm; fig. S5A). We then assessed cellular recruitment into the gel layer of microneedles carrying pam3Cys (either free or encapsulated in ICMVs) together with polyI:C in the alginate coating. As shown in fig. S5B, incorporation of pam3Cys and polyI:C into the alginate coating increased cellular infiltration into the microneedle, and incorporation of pam3Cys into ICMVs further enhanced cell recruitment ~8-fold over microneedles carrying free pam3Cys. ICMV nanocapsules have a high degree of stability under physiological conditions, showing very low loss of encapsulated cargo over several days in the presence of serum (*20*). As shown in fig. S6A, there was no significant drop in the quantity of polyI:C recovered from microneedles after 24-hour application to murine ear skin,

and polyI:C recovered from microneedles stimulated TLR3-expressing reporter cells in culture similarly to polyI:C extracted from as-fabricated patches (fig. S6B). Thus, the polyI:C adjuvant is stable over the duration of sampling in vivo.

Inclusion of antigen in the sampling layer enhances recovery of antigen-specific lymphocytes by sampling microneedles

Incorporation of adjuvants in the gel layer should promote nonspecific recruitment of leukocytes, but such nonspecific cell sampling does not reflect the enrichment of antigen-specific lymphocytes that occurs rapidly at a site of infectious challenge (*25*). Thus, we next introduced specific antigens into ICMVs carried in the gel coating, coencapsulating pam3Cys and the model antigen OVA to generate SSMNs. Dendritic cells can cross-present exogenous protein antigen to $CD8^+$ T cells within a few hours of uptake (*26*). As illustrated in Fig. 1A, our expectation was that APCs taking up antigen in the alginate matrix would present peptides in situ to recruited antigen-specific T cells, arresting their migration and egress from the alginate matrix in response to T cell receptor signaling and thereby enriching for antigen-specific cells in the sampled cell population.

To test this idea, SSMNs were prepared with alginate coatings carrying polyI:C and ICMVs coloaded with pam3Cys and OVA. SSMNs were applied for 12, 24, or 48 hours on the ears of OVA-immunized mice. These SSMN sampling groups were compared to animals sampled by a Mantoux-type experiment, where antigen and adjuvant were injected intradermally 60 hours before application of microneedles carrying no stimuli in the alginate coating (Fig. 3A, SMNs). As shown in Fig. 3 (B and C), 12-hour application of SSMNs to the skin of mice receiving no pretreatment recovered total live cells and $CD8^+$ T cells in numbers comparable to alginate-only SMNs applied in the two-step "Mantoux" setting. Application of SSMNs for 24 hours increased the cell recovery by another ~3-fold, whereas sampling for 48 hours increased cell recovery by ~8 fold (Fig. 3, B and C). On average, ~9 to 10 times more OVA-specific T cells were retrieved by SSMNs applied for 24 hours compared to 12 hours, with only a minor further gain in OVA-specific cells for a 48-hour application time (Fig. 3, D and E). Microneedles applied for 24 hours maximized the recovery of $CD3^+CD8^+CD69^+CD103^+$OVA-specific T_{RM} cells (Fig. 3, F and G). Among OVA-specific T cells, we noted that a longer SSMN application time resulted in the recovery of more T cells recruited from the systemic circulation and a decreasing proportion of OVA-specific T_{RM}s (Fig. 3G). On the basis of these findings, we chose to focus on 24-hour SSMN sampling times to maximize T_{RM} sampling.

We next evaluated how antigen inclusion in the cell sampling layer affected the composition of recovered leukocytes. As expected, antigen-loaded microneedles not only were more effective in recovering antigen-specific T cells but also led to a generally higher recovery of total leukocytes (Fig. 4, A to E). This may reflect rapid activation of antigen-specific T_{RM}s recruited to the microneedles, which would both arrest these cells in the gel layer and trigger production of additional cytokines/chemokines (*27*). We next titrated the dose of OVA incorporated in the microneedles, holding the adjuvant dose constant (Fig. 4F). A notable increase in recovered antigen-specific and nonspecific T cells was observed when the microneedles carried 2 μg of OVA compared to the lower doses of antigen (Fig. 4, G to J). About 5000 live cells were typically recovered from a single microneedle array loaded with 2 μg of antigen. On the basis of these studies, a 24-hour application with cell sampling microneedles incorporating 2 μg of antigen in ICMVs in the cross-linking layer of the alginate coating was designated as the optimized sampling strategy.

Confocal microscopy of SSMNs after skin sampling of OVA-immunized eGFP mice showed the presence of cells infiltrating the alginate matrix in close proximity to aggregates of ICMV particles (Fig. 5A). Scanning electron microscopy also revealed lymphoid cells displaying lamellar protrusions embedded within the matrix, which were absent in control samples containing neither antigen nor adjuvant (Fig. 5, B and C). To determine whether infiltrating APCs interacted with ICMVs embedded within the alginate layer, we used an image-based cytometry methodology: Cells recovered by SSMNs were seeded in a nanowell array, stained with antibodies, and subsequently imaged by high-throughput microscopy (Fig. 5D). Imaging cytometry analysis showed that 20% of cells recovered from OVA-immunized mice were T cells ($CD3e^+$), 15% were $CD19^+$ B cells, and ~20% of recovered cells were $CD45^+CD3e^-CD19^-CD11c^+$, likely APCs, with the remaining cells likely myeloid cells and granulocytes (Fig. 5E). Micrographs of individual nanowells containing single cells showed live APCs that were positive for both ICMVs and fluorescent OVA signals, suggesting an uptake of OVA-ICMVs by recruited dendritic cells in the gel layer (Fig. 5F). Essentially, all $CD11c^+$ APCs recovered from the microneedles were $ICMV^+$ (Fig. 5G). In addition, among $MHCII^+$ APCs recovered from SSMNs, the expression of the activation markers CD40 and CD86 was considerably increased compared to cells recovered from unstimulated ear skin or cells sampled with microneedles containing no antigen/adjuvants (Fig. 5, H and I, and fig. S7). Thus, relevant APCs efficiently acquired the antigen- and adjuvant-loaded nanocapsules and become activated on infiltration into the sampling microneedle matrix.

SSMNs do not immunize animals during sampling

A potential concern with SSMNs is that recruited APCs might carry antigen from the microneedle matrix to draining lymph nodes, thereby immunizing the recipient and altering their immune status by the act of sampling. To test whether microneedle sampling immunizes animals, the skin of naïve mice was sampled with optimized SSMNs carrying adjuvants (polyI:C and pam3cys) and OVA-ICMVs (Fig. 6A). As shown in Fig. 6B, OVA-specific $CD8^+$ T cells in the blood remained undetectable before and after sampling. As a positive control, the animals were subsequently vaccinated at 24 days after sampling with OVA in adjuvant, and 7 days later, a clear $tetramer^+CD8^+$ T cell population appeared in the blood. We also tested the more sensitive setting of animals having pre-existing memory T cells by sampling the skin of OVA-immunized mice. Again, no significant difference was found in the frequency of antigen-specific $CD8^+$ T cells in the blood before and after sampling (Fig. 6C). Extending the SSMN application time to 48 hours also did not immunize the animals, as shown in fig. S8.

Antibody responses can often be elicited by low doses of antigen reaching lymph nodes even under conditions where cross-presentation of antigen to $CD8^+$ T cells is negligible. We thus next assessed whether SSMNs induced changes in serum antibody titers against antigens carried in the microneedle gel matrix in the naïve or preimmune settings. As shown in Fig. 6D, serum OVA-specific IgG titers showed no change before and after sampling with microneedles carrying OVA-ICMVs, whether applied to naïve or OVA-immunized animals. Thus, sampling of cells/ISF from the skin by SSMNs does not appear to immunize or alter pre-existing T cell or B cell responses against target antigens.

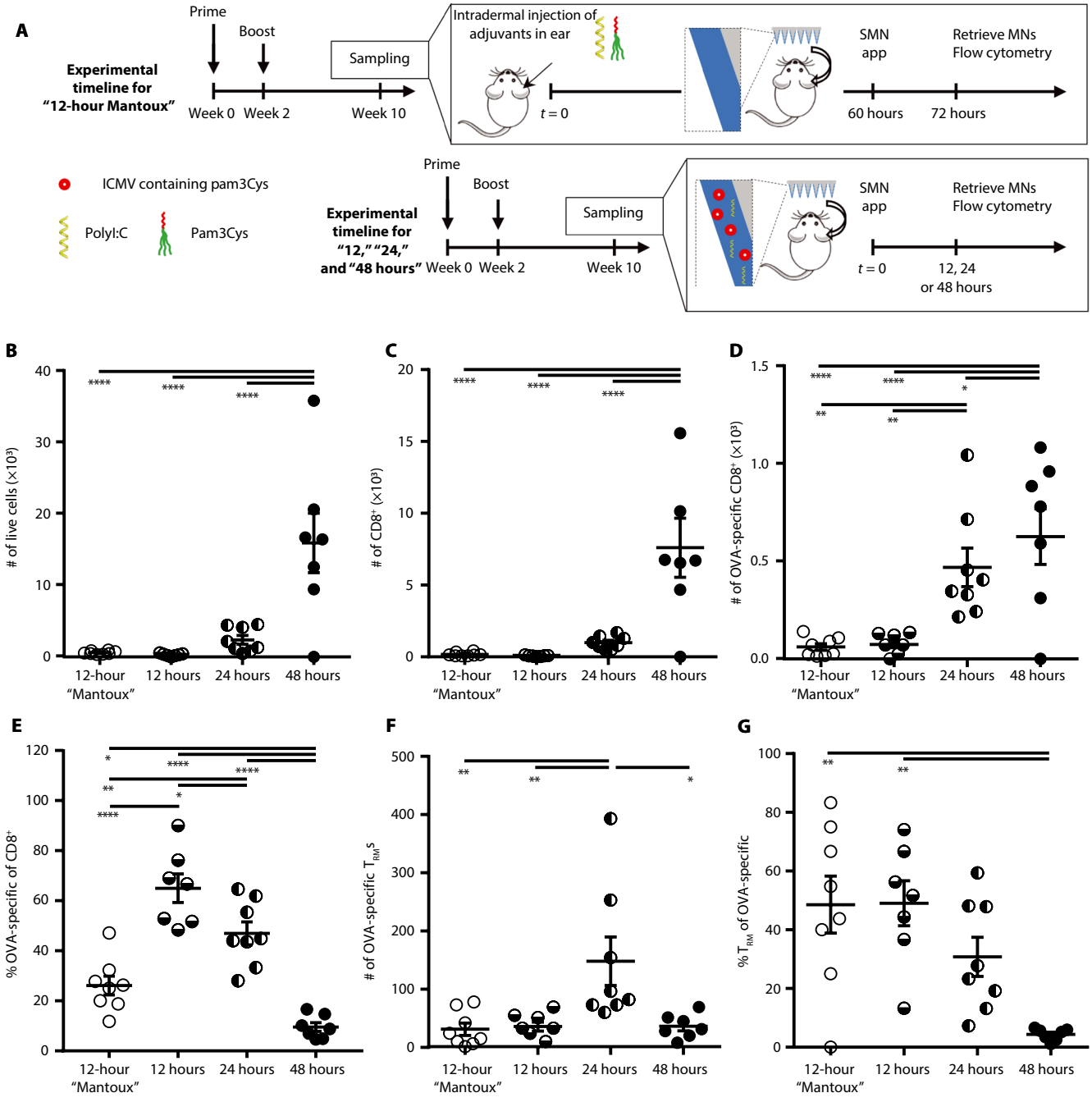

Fig. 3. Microneedles incorporating adjuvants enable single-step sampling of antigen-specific T_{RM}s. (**A**) Timeline of sampling optimization in C57Bl/6 mice ($n = 5$ per group). (**B** to **G**) Enumeration of recovered total live cells (B), $CD8^+$ T cells (C), OVA-specific $CD8^+$ T cells (D), frequency of OVA-specific cells (E), OVA-specific T_{RM}s (F), and frequency of T_{RM}s among OVA-specific cells (G). Cell counts are per microneedle patch. Data shown are means ± SEM from one representative of three independent experiments. *$P < 0.05$, **$P < 0.01$, and ****$P < 0.0001$, analyzed by one-way ANOVA, followed by Tukey's HSD.

Sampling microneedles allow longitudinal monitoring of T_{RM}s

Having optimized the sampling microneedle platform, we lastly sought to demonstrate the capacity of this approach to follow T_{RM} populations in the skin of animals longitudinally. Mice were primed and boosted with OVA and adjuvant, and then, skin-resident immune populations were tracked at 2 to 70 weeks after boost. As expected, the proportion of SIINFEKL tetramer$^+$ (OVA-specific) $CD8^+$ T cells in the blood decreased sharply in 10 weeks after the boost, plateauing to a stable population of circulating memory cells (Fig. 7, A and B). In contrast, SSMNs revealed a tissue-resident population of antigen-specific T cells that decayed slightly over the same 10-week post-boost period and then remained roughly constant for the next 60 weeks. The number of T_{RM}s and OVA-specific T_{RM}s also remained unchanged after sampling via SSMNs (Fig. 7, C and D).

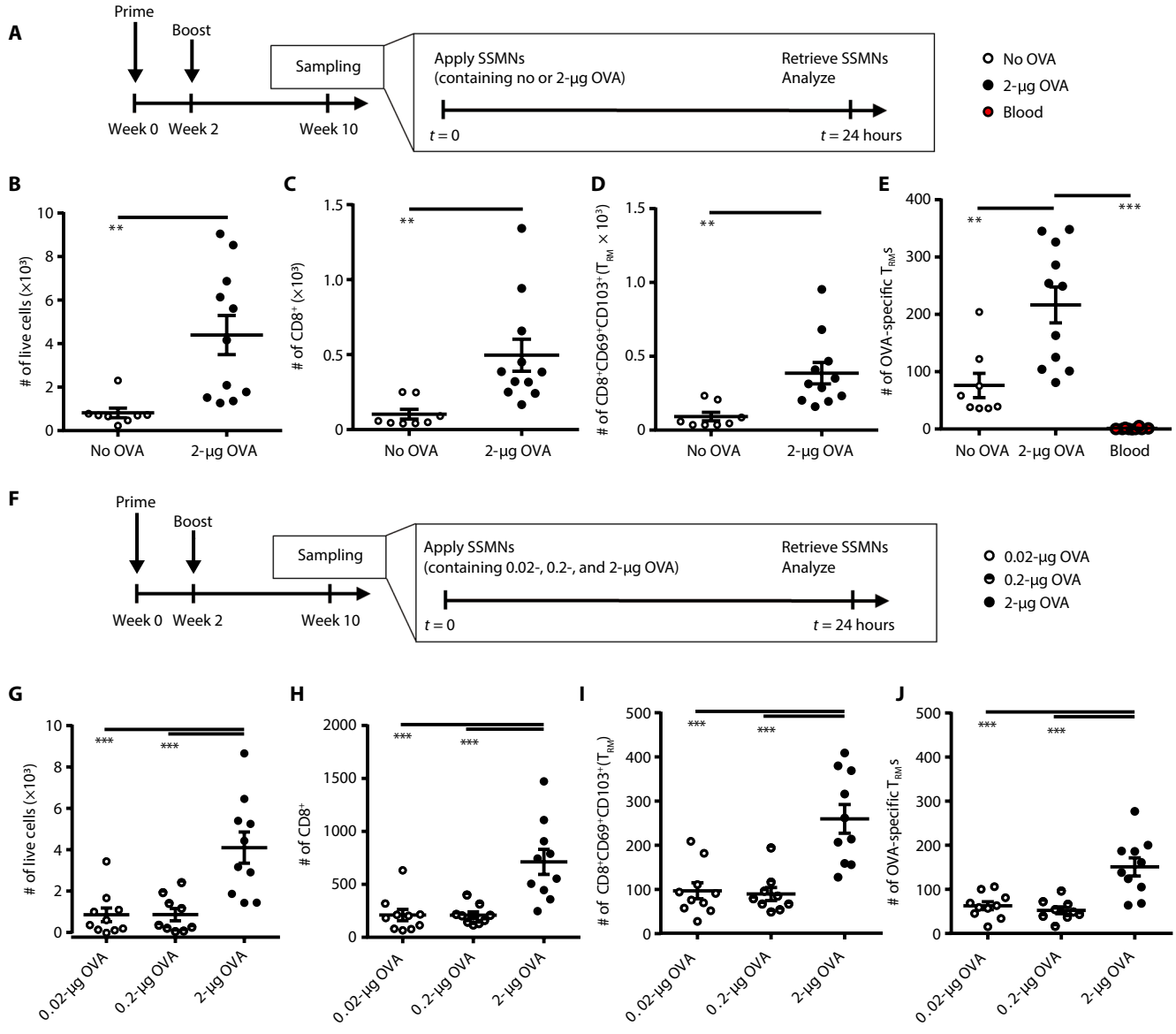

Fig. 4. SSMNs containing antigen-loaded nanocapsules enrich sampling for antigen-specific T_{RM}s. (**A** to **E**) Groups of OVA-immunized C57Bl/6 mice ($n = 6$ per group) were sampled with SSMN arrays applied to the ear according to the timeline (A). Enumeration of recovered total live cells (B), $CD8^+$ T cells (C), $CD8^+CD69^+CD103^+$ T_{RM}s (D), and OVA-specific T_{RM}s (E), per SSMN array, from SSMNs containing empty ICMV nanocapsules or ICMVs loaded with 2 μg of OVA. (**F** to **J**) Groups of OVA-immunized C57Bl/6 mice ($n = 5$ per group) were sampled with microneedles applied to the ear according to the timeline (F). Enumeration of recovered total live cells (G), $CD8^+$ T cells (H), $CD8^+CD69^+CD103^+$ T_{RM}s (I), and OVA-specific T_{RM}s (J), per SSMN array, from SSMNs containing ICMVs encapsulating 0.02, 0.2, or 2 μg of OVA. Data shown are means ± SEM from one representative of two to three independent experiments. $^{**}P < 0.01$, $^{***}P < 0.001$, analyzed by one-way ANOVA, followed by Tukey's HSD.

We next evaluated SSMNs for measuring T_{RM}s after a live infectious challenge. Mice were infected with vaccinia virus expressing SIVgag via tail skin scarification (*28*). SSMNs were prepared, incorporating ICMV nanocapsules loaded with gag peptide, and cells were sampled from ear skin of the mice at 11 weeks after infection. The microneedle platform detected T_{RM}s and gag-specific T_{RM}s, which were not present in the blood (Fig. 7, E to H). The frequency of antigen-specific $CD8^+$ T cells both in the skin (sampled via microneedles) and in systemic circulation (sampled via blood) was lower than that in OVA-immunized mice, because the skin scarification model is a weaker form of antigen exposure than intradermal immunization. However, similar to the OVA model, SSMNs detected a stable skin-resident antigen-specific T cell population that was completely absent from the blood a few months after infection (Fig. 7, I to K). Thus, SSMNs can report longitudinally on skin-resident memory cell populations not detectable in the systemic circulation.

Immune cells can be sampled from human skin explants

We finally performed proof-of-concept studies to test microneedle sampling from human skin, which is thicker than mouse skin. Sampling microneedles, similar to those used in murine studies, with or

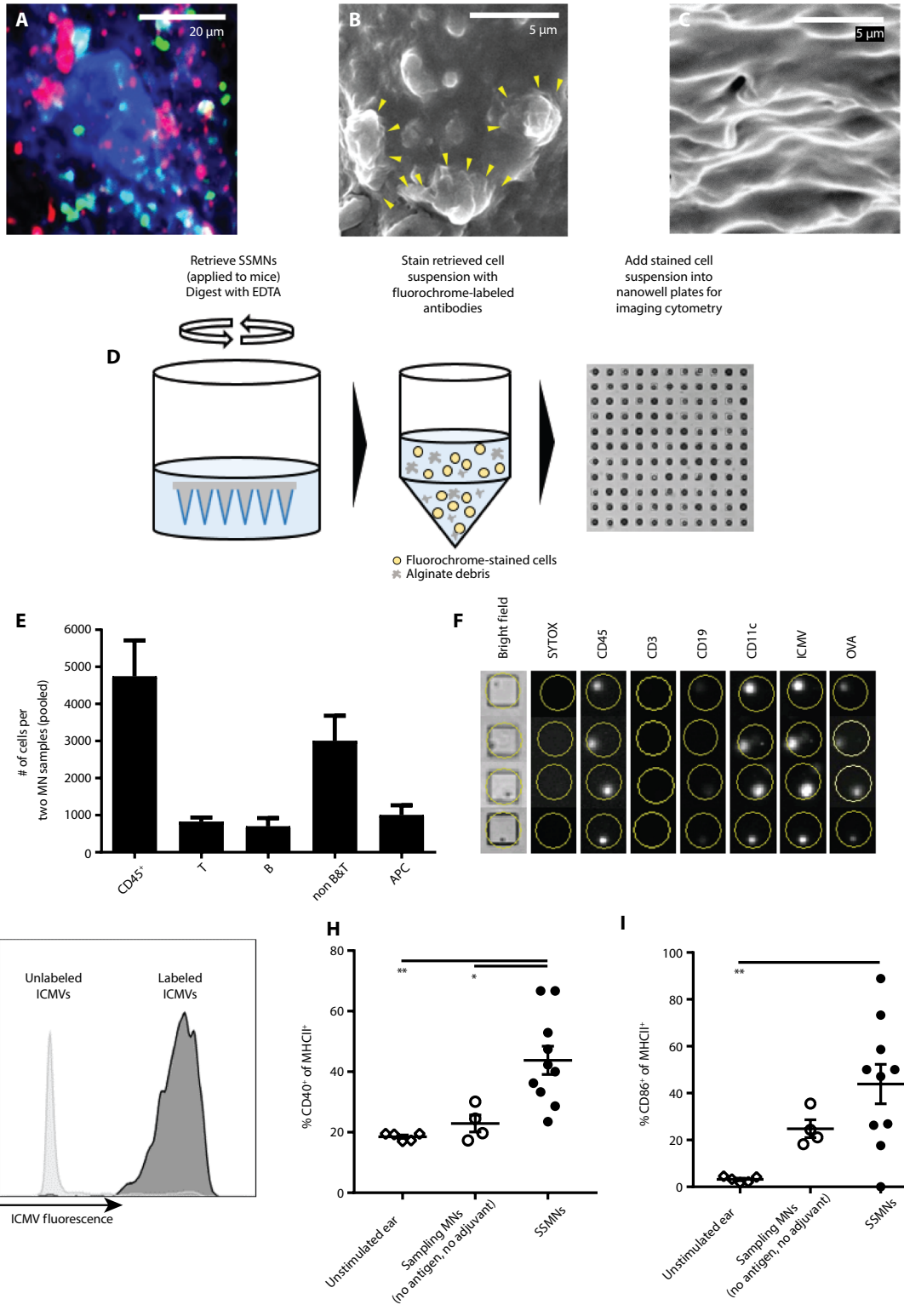

Fig. 5. Sampling microneedles containing ICMV nanocapsules accumulate antigen-loaded dendritic cells. (**A**) Confocal micrograph of SSMN array surface showing alginate (blue), embedded ICMVs (pink), and recruited cells (green), after application to the skin of eGFP mice. (**B**) Scanning electron microscopy image of SSMNs after application to mouse skin for 24 hours showing lymphocytes, about 5 μm in diameter (**C**). (**D** to **G**) SSMNs containing 5 μg of polyI:C-labeled ICMVs encapsulating 2 μg of Alexa Fluor 555–labeled OVA and 5 μg of pam3Cys were applied to the ears of OVA-immunized mice ($n = 3$ per group) for 24 hours, followed by retrieval, antibody staining, and phenotypic analysis via imaging cytometry (D). (E) Cell phenotypes obtained from SSMNs. (F) Representative imaging cytometry data showing overlay of fluorescent channels for live/dead dye Sytox, CD45, CD3, CD19, CD11c, ICMV, and OVA–Alexa Fluor 555. Dimension of each well is 50 μm. (G) Representative two-dimensional imaging cytometry plots showing OVA/ICMV fluorescence in $CD45^+CD11c^+$ dendritic cells. (**H** and **I**) Expression of activation markers CD40 (H) and CD86 (I) among APCs recovered by microneedles. Data shown are means ± SEM from one representative of two to three independent experiments. $^*P < 0.05$, $^{**}P < 0.01$, analyzed by one-way ANOVA, followed by Tukey's HSD.

without incorporated adjuvants were applied to fresh human skin obtained from abdominoplasty surgeries for 16 hours, maintaining the samples in a humid chamber at 37°C (Fig. 8A). Immunophenotyping via flow cytometry of sampled cells mirrored findings from the murine studies: Microneedles containing adjuvants sampled several thousand live cells per patch from human skin and increased the number of $CD8^+$ and $CD11c^+$ cells recovered, compared with microneedles without adjuvants (Fig. 8, B to D, and fig. S9). These results suggest that SSMNs are suitable for minimally invasively sampling of immune cell populations in human skin.

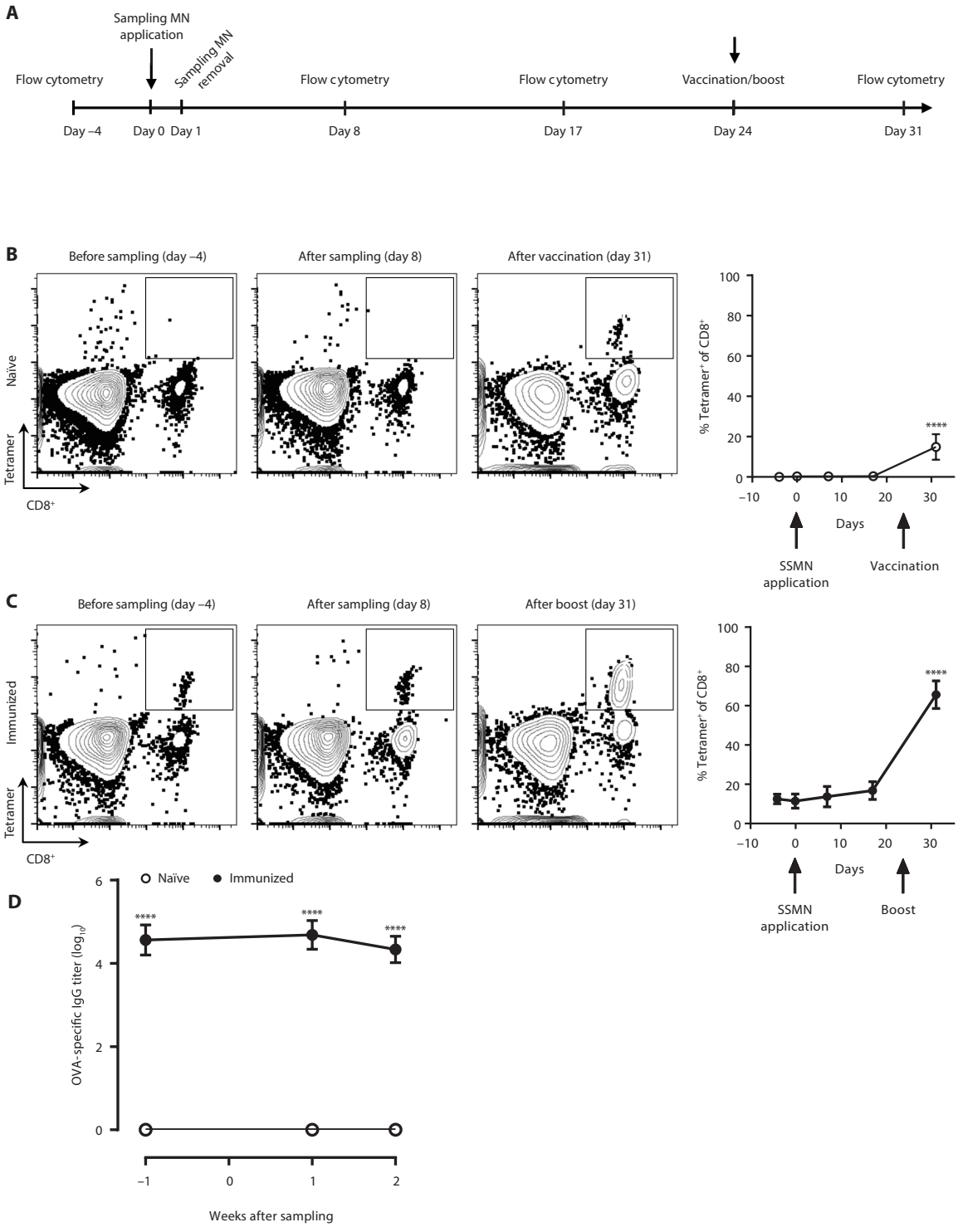

Fig. 6. Sampling microneedles do not change the immune status of the animal. SSMN arrays containing adjuvants and ICMVs loaded with 2 μg of OVA were applied to the ears of naïve or OVA-immunized C57Bl/6 mice, immunized 8 to 10 weeks before (n = 5 per group) for 24 hours and then retrieved and analyzed via flow cytometry. The experimental timeline (**A**), representative flow cytometry plots, and quantification of OVA-specific $CD8^+$ T cells from the blood in naïve (**B**) and previously immunized (**C**) mice, before and after SSMN application at day 0 and vaccination on day 24 are shown. (**D**) Serum OVA-specific IgG titers before and after sampling with SSMNs. Data shown are means ± SEM from one representative of two independent experiments. ****$P < 0.0001$ analyzed by one-way ANOVA, followed by Tukey's HSD.

DISCUSSION

Recent studies have identified key roles for tissue-resident immune cells. T_{RM}s in particular have been revealed as critical players in immunity, even in the absence of ongoing antigen presentation. T_{RM}s in both mice and humans have been implicated in immune protection in the lungs, skin, gut, and other mucosal linings, enhancing immunity to both infections and tumors (*27*). Investigation of T_{RM}s and their function in small animal models is usually achieved by sacrificing cohorts at defined time points to harvest their tissue or by obtaining invasive biopsies from larger animals and humans because T_{RM}s cannot be obtained from traditional blood draws.

Here, we present a microneedle-based, minimally invasive system for monitoring tissue-resident immune cells. This microneedle sampling platform enables isolation of live immune cells from the

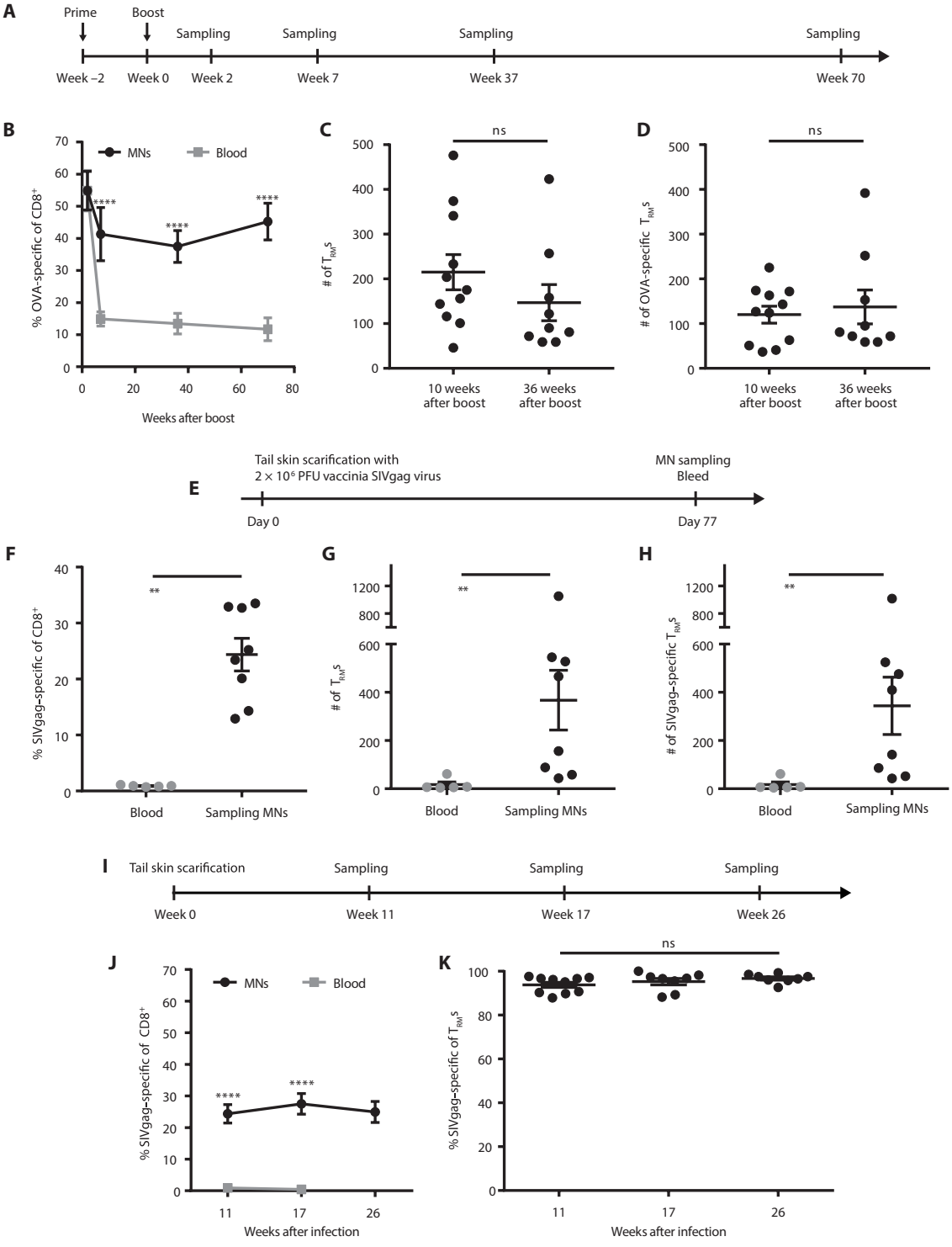

Fig. 7. Sampling microneedles reveal a stable population of T_{RM}s in skin up to a year after vaccination or infection. (**A** to **D**) Groups of C57Bl/6 mice ($n = 5$ per group) were primed and boosted with OVA and adjuvant and then repeatedly sampled using SSMN arrays and blood draws over time. (A) Timeline. (B) OVA-specific $CD8^+$ T cells over time. (C and D) T_{RM}s (C) and OVA-specific T_{RM}s (D) quantified from SSMNs and the blood. (**E** to **H**) Groups of C57Bl/6 mice ($n = 5$ per group) were infected with 2×10^6 PFU (plaque-forming units) of SIVgag-expressing vaccinia virus via tail skin scarification and sampled beginning 11 weeks after infection via blood draws or SSMNs applied to the ear containing ICMVs (2 μg of AL11 SIVgag peptide and 5 μg of pam3Cys) and 5 μg of polyI:C. After 24 hours, patches were retrieved and analyzed via flow cytometry. Experimental timeline (E), frequency of SIVgag tetramer$^+$$CD8^+$ T cells (F), enumeration of $CD8^+CD69^+CD103^+$ T_{RM}s (G), and SIVgag-specific T_{RM}s (H) from the blood and SSMNs. (**I** to **K**) Timeline (I), frequency of SIVgag-specific $CD8^+$ T cells (J), and frequency of SIVgag-specific T_{RM}s (K) when sampled at various times after vaccinia infection. Data shown are means ± SEM from one representative of two to three independent experiments. $^{**}P < 0.01$ and $^{****}P < 0.0001$, analyzed by Wilcoxon-Mann-Whitney test (F to H), one-way ANOVA (K), or two-way ANOVA (B and J).

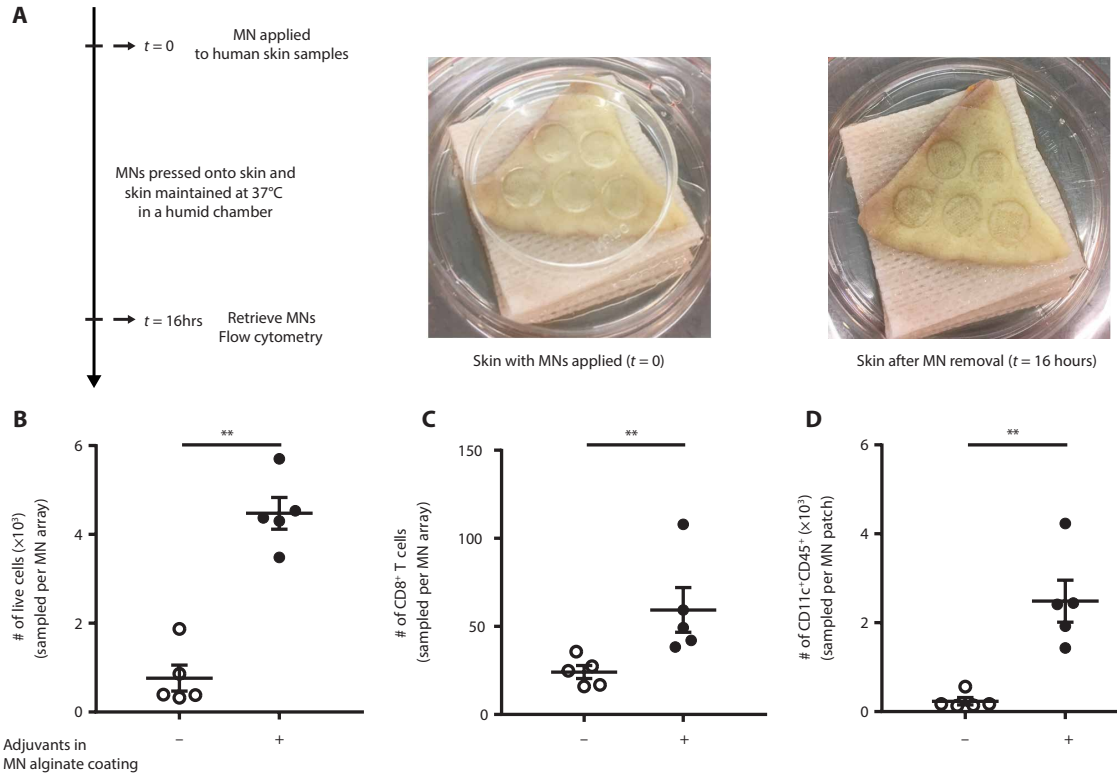

Fig. 8. SSMNs enable sampling of lymphocytes from human skin. Five SSMN arrays each were applied to excised human skin samples from $n = 5$ donors for 16 hours, and then gel coatings were digested for analysis of recovered cells via flow cytometry. (**A**) Timeline and photographs of the experimental setup. (**B** to **D**) Enumeration of recovered total live cells (**B**), $CD8^+$ T cells (**C**), and $CD11c^+CD45^+$ cells (**D**), per sampling microneedle array, from microneedles containing no adjuvants or from SSMNs containing polyI:C and ICMVs encapsulating pam3Cys. Data shown are means ± SEM from two independent experiments, with samples obtained from five total donors. $^{**}P < 0.01$, analyzed by two-tailed nonparametric Mann-Whitney test.

skin, as well as ISF and biomarkers contained within it. By incorporating specific antigens within nanocapsules embedded within the cell sampling alginate layer, SSMNs become a micro-Mantoux test and minimally invasive biopsy in one, allowing target lymphocyte populations of interest to be enriched in the sampled population, mimicking the response to a genuine infectious challenge. Sampling microneedles take the qualitative output of a classical delayed-type hypersensitivity/Mantoux test and could enable deep phenotypic and functional profiling of the responding antigen-specific tissue infiltrates. The ability to isolate live cells permits longitudinal analysis of functional traits of lymphocytes from the same animal/individual, traditional phenotyping, or advanced genomic methods such as single-cell RNA sequencing. Optimized SSMNs enabled ~2500 leukocytes to be recovered from a single 1-cm-diameter patch after a 24-hour application.

Key to this approach was the identification of a microneedle design that could be infiltrated by cells but could retain sufficient mechanical integrity to withstand the mechanical forces of skin insertion. With an ultimate goal of low-cost, safe, disposable patches, we focused on microneedles fabricated from melt-molded bioresorbable polymers. In preliminary studies, we found that porous polymer microneedles did not have sufficient mechanical integrity for skin insertion, consistent with the rapid decline in modulus of materials as volume percent porosity increases. By using a dehydrated hydrogel coating over a solid "core" microneedle substrate, we were able to arrive at a composition with a stable stiff surface layer during skin insertion, which could swell to provide a porous matrix amenable to cell infiltration in situ.

Sampling microneedles carrying no stimulus in the hydrogel layer could recover lymphocytes for analysis, likely attracted to the patch in response to cell death and cytokines/chemokines produced in response to the local physical microtrauma of microneedle insertion (*29*). However, we incorporated specific antigens and adjuvants into the sampling layer to both increase the number of recovered cells and more completely mimic cellular recruitment elicited by an infectious challenge, where both antigen and danger signals would naturally be present. Incorporation of adjuvants into the gel layer increased cell recovery by twofold over "empty" alginate coatings, and introduction of specific antigens further increased this recovery by another ~4.5-fold in immunized animals.

Microneedles that release antigen and adjuvant into skin tissue are well known to effectively prime immune responses in vivo (*18*, *30*, *31*). In response to inflammatory cues, Langerhans cells, dermal dendritic cells, and other APCs either resident or recruited to the skin will become activated, leading to up-regulation of chemokine receptors that guide their migration to lymphatic vessels and draining lymph nodes, where captured antigen is presented to lymphocytes (*32*). We sought to circumvent this natural process during microneedle sampling by encapsulating our stimulatory antigen in nanocapsules physically entrapped within the alginate layer to avoid dissemination of antigen into the surrounding tissue after microneedle application. SSMNs delivering small but non-negligible quantities

of antigen/adjuvant did not lead to detectable priming of antigen-specific T cells or antibody responses in treated mice, even if the animals had pre-existing memory populations against the sampling antigen. The fact that patch application for up to 48 hours did not stimulate an immune response suggests that APCs recruited to the microneedle coating are unable to migrate back out of the gel layer. We hypothesize that cells recruited into the alginate layer are shielded from chemokines produced by lymphatics that normally guide APCs to the draining lymph nodes, effectively trapping them in the microneedle coating.

A limitation with collecting cell and/or ISF samples using sampling microneedles includes the size of the sample and possible limit-of-detection issues for methods that depend on high analyte concentrations. On average, ~5000 live cells including ~2500 leukocytes are obtained per microneedle array (1 cm^2) and about 1 to 2 μl of ISF. Of course, increasing the size of the microneedle array will linearly increase the sample size. In addition, with regard to safety considerations after microneedle application, similar to the findings of other studies (*33*), the area of sampling microneedle application in our studies also healed within 2 to 3 days, with only minor erythema and inflammation for the first 24 to 48 hours.

We expect that microneedle immune monitoring can affect at least three major areas of medicine: (i) enabling better disease management in autoimmune conditions by predicting oncoming disease flares, (ii) monitoring tissue status in transplantation, and (iii) monitoring vaccine responses. Methods for monitoring autoimmune diseases rely primarily on blood draws. However, cutaneous disorders such as lupus or psoriasis may be better served by biomarkers directly obtained from the skin. It is known that, although ~83% of serum proteins are found in ISF, 50% of the proteins found in ISF are found in the ISF alone, and not in serum (*21*). Being able to sample for biomarkers from skin, in a painless and minimally invasive manner, without the need of trained personnel for fluid withdrawal, could enable more granular flare prediction. In transplantation, recent work monitoring local reactions to skin transplants has suggested that donor T_{RM}s show early accumulations in allografts that will be rejected (*34*). A minimally invasive means to monitor for such reactions and preemptively provide immunosuppressive interventions could increase the lifetime of these grafts. Last, as shown here in our preclinical models, T_{RM} responses established by vaccination can be readily monitored with SSMNs. We focused here on skin immune monitoring because of its importance for autoimmunity, transplants, and vaccines against bacterial and mosquito-borne pathogens, but microneedles have been used at many other mucosal sites such as buccal (*35*) and vaginal (*36*) surfaces, as well as applied to cutaneous tumors (*37*). We thus expect microneedle sampling to be relevant for many other applications beyond immune monitoring in the skin.

MATERIALS AND METHODS

Study design

The objective of this study was twofold: first, to sample T_{RM} populations, not found in blood, from skin, via a minimally invasive skin patch, incorporating microneedles; and second, to assess the quantification of commonly found biomarkers in blood, for example, antigen-specific IgG, as detected in ISF collected by microneedles. All in vivo studies involving flow cytometry analysis were carried out in C57BL/6 mice, randomized into groups of four or more mice per treatment. Primary data are reported in table S1.

Mice

Animal studies were approved by the Massachusetts Institute of Technology (MIT) Institutional Animal Care and Use Committee (protocol number 0717-076-20), and animals were cared for in the U.S. Department of Agriculture–inspected MIT Animal Facility under federal, state, local, and National Institutes of Health guidelines for animal care. Female C57BL/6 mice (3 to 6 weeks of age) and C57Bl/6 mice expressing GFP under control of the ubiquitin promoter were obtained from the Jackson Laboratory, and the colonies were maintained at the animal Koch Institute mouse facility at MIT.

Fabrication of alginate-coated microneedles

PMDS molds (Sylgard 184, Dow-Corning) for fabrication of microneedle arrays were prepared by laser micromachining (*38*). Poly-L-lactide (PLLA; RESOMER L 207 S, Evonik Industries AG) was melted over the molds under vacuum (−20 mmHg, 200°C, 40 min). Poly-L-lysine (0.01 wt %; P4832, Sigma-Aldrich) solution was pipetted onto PLLA microneedles for 30 min, the solution was removed after 30 min, and the microneedles were dried at 25°C. Alginate (PRONOVA SLG100 or PRONOVA SLM20, FMC BioPolymer) and sucrose (Sigma-Aldrich) solution (0.35 mg of alginate, 1.4 mg of sucrose in 60 μl of water) was pipetted onto each PLLA microneedle array and dried under vacuum at 25°C for at least 4 hours. Cross-linking solution containing ICMV particles and polyI:C (average size, 1.5 to 8 kb, 5 μg; HMW, InvivoGen) and calcium (0.1 mg) in total volume of 50 μl was pipetted onto the surface of microneedles and dried under vacuum for >12 hours.

Skin application of microneedles

Animals were anesthetized using isofluorane, and ears of the mice were laid out flat on 3M Nexcare waterproof tape. Alginate-coated microneedles, with or without cargo of antigen and/or adjuvant in the gel coating, were applied by pressing down vertically with the thumb or index finger while securing Nexcare tape around the microneedle to keep it securely in place. Another layer of waterproof tape was secured around the first layer to keep the microneedle application site dry during the application period.

Processing of cells from gels and microneedles and flow cytometry

Subcutaneously injected gels were mashed using the backside of a syringe plunger and digested with alginate lyase (1 mg/ml; A1603, Sigma-Aldrich) and EDTA [0.02% of a stock solution (pH 5.5)] for 45 min at 37°C with intermittent pipetting to break up the gel further. The solution was strained through at 50-μm cell strainer and pelleted. Frequencies of live cells were determined after staining with 4′,6-diamidino-2-phenylindole. Each alginate-coated microneedle retrieved from mouse ears was immersed in 200 μl of PBS containing 1% bovine serum albumin and 100 mM EDTA and incubated at 37°C on a shaker at 150 rpm for 30 min. The supernatant was collected and centrifuged to pellet cells. Recovered cells were resuspended in 100 μl of 0.36 μM CFSE in PBS for 5 min at 25°C for staining, quenched with 150 μl of RPMI containing 10% fetal bovine serum for 15 min, and washed. Frequencies of antigen-specific $CD8^+$ T cells and their phenotypes were determined by flow cytometry analysis of labeled cells after staining with anti-mouse antibodies (CD8α APC/Cy7, CD69 PE/Cy5, and CD103 BV421) from BioLegend and SIINFEKL/H-$2K^b$ peptide–MHC (major histocompatibility complex) tetramer [iTAg Tetramer/PE–H-$2K^b$ OVA (SIINFEKL) from MBL

International] or SIVgag tetramer [iTAg Tetramer/PE–H-2D^b SIV GAG (AAVKNWMTQTL) from MBL International] using a BD FACSCelesta HTS-1.

Human skin experiments

Ethics statement

Healthy human skin tissue was obtained from abdominoplastic surgery. The studies were approved by the respective institutional review boards [National Health Group Domain Specific Review Board (NHG DSRB 2012/00928) and SingHealth Centralised Institutional Review Board (CIRB 2011/327/E), respectively], and patients gave written informed consent. All skin samples were processed on the day of surgery.

Microneedle patch application to explanted skin tissue

Microneedles were applied to explanted human skin samples, and adherence was maintained using a small petri dish to provide downward pressure. These skin samples were maintained in a humid chamber for 16 hours at 37°C, as shown in Fig. 8A.

Flow cytometry

CellTrace CFSE (C34554, Thermo Fisher Scientific), CountBright absolute counting beads (C36950, Thermo Fisher Scientific), CD3 APC (UCHT1, BioLegend), CD4 PE (RPA-T4, BioLegend), CD8 AF700 RPA-T8, BioLegend), CD45 V500 (HI30, BD Horizon), HLA-DR PECy7 (L243, BD Pharmingen), CD11c V450 (B-Ly6, BD Horizon), and CD14 PerCPCy5.5 (HCD14, BioLegend) were used for flow cytometry analysis.

Statistical analysis

Datasets were analyzed using two-tailed nonparametric Mann-Whitney test, one- or two-way ANOVA tests, followed by Tukey's HSD test for multiple comparisons with Prism (GraphPad Software). *P* values less than 0.05 were considered statistically significant. All values are reported as means ± SEM.

SUPPLEMENTARY MATERIALS

www.sciencetranslationalmedicine.org/cgi/content/full/10/467/eaar2227/DC1
Materials and Methods
Fig. S1. Optimization of alginate coating composition.
Fig. S2. Analysis of fluids recovered from microneedles accurately reflects surrounding solution concentrations.
Fig. S3. T_{RM} characterization in the blood and skin compartments in OVA-immunized mice.
Fig. S4. Cell recruitment is enhanced with the inclusion of adjuvants in the alginate hydrogel coating.
Fig. S5. ICMV characterization and increased recruitment of cells into sampling microneedles when ICMVs encapsulating antigen and adjuvant are embedded in the alginate layer of sampling microneedles.
Fig. S6. The activity of polyI:C is retained upon incorporation within sampling microneedles.
Fig. S7. SSMNs containing adjuvants activate recruited APCs.
Fig. S8. SSMN application for up to 48 hours does not change the immune status of the animal.
Fig. S9. Gating strategy for cells obtained from sampling microneedles applied to human skin.
Table S1. Primary data.
Reference (*39*)

REFERENCES AND NOTES

1. L. A. Parapia, History of bloodletting by phlebotomy. *Br. J. Haematol.* **143**, 490–495 (2008).
2. M. Streitz, T. Miloud, M. Kapinsky, M. R. Reed, R. Magari, E. K. Geissler, J. A. Hutchinson, K. Vogt, S. Schlickeiser, A. H. Kverneland, C. Meisel, H.-D. Volk, B. Sawitzki, Standardization of whole blood immune phenotype monitoring for clinical trials: Panels and methods from the ONE study. *Transplant. Res.* **2**, 17 (2013).
3. V. Srinivasan, V. Pamula, M. Pollack, R. Fair, Clinical diagnostics on human whole blood, plasma, serum, urine, saliva, sweat, and tears on a digital microfluidic platform. *Proc. MicroTAS* 1287–1290 (2003).
4. E. G. Perdiguero, F. Geissmann, The development and maintenance of resident macrophages. *Nat. Rev. Immunol.* **17**, 2–8 (2016).
5. Y. He, M. Shimoda, Y. Ono, I. B. Villalobos, A. Mitra, T. Konia, S. A. Grando, J. J. Zone, E. Maverakis, Persistence of autoreactive IgA-secreting B cells despite multiple immunosuppressive medications including rituximab. *JAMA Dermatol.* **151**, 646–650 (2015).
6. D. K. Sojka, B. Plougastel-Douglas, L. Yang, M. A. Pak-Wittel, M. N. Artyomov, Y. Ivanova, C. Zhong, J. M. Chase, P. B. Rothman, J. Yu, J. K. Riley, J. Zhu, Z. Tian, W. M. Yokoyama, Tissue-resident natural killer (NK) cells are cell lineages distinct from thymic and conventional splenic NK cells. *eLife* **3**, e01659 (2014).
7. E. M. Steinert, J. M. Schenkel, K. A. Fraser, L. K. Beura, L. S. Manlove, B. Z. Igyártó, P. J. Southern, D. Masopust, Quantifying memory CD8 T cells reveals regionalization of immunosurveillance. *Cell* **161**, 737–749 (2015).
8. R. Watanabe, A. Gehad, C. Yang, L. L. Scott, J. E. Teague, C. Schlapbach, C. P. Elco, V. Huang, T. R. Matos, T. S. Kupper, R. A. Clark, Human skin is protected by four functionally and phenotypically discrete populations of resident and recirculating memory T cells. *Sci. Transl. Med.* **7**, 279ra39 (2015).
9. L. K. Beura, D. Masopust, Snapshot: Resident memory T cells. *Cell* **157**, 1488–1488.e1 (2014).
10. M. Vukmanovic-Stejic, J. R. Reed, K. E. Lacy, M. H. A. Rustin, A. N. Akbar, Mantoux test as a model for a secondary immune response in humans. *Immunol. Lett.* **107**, 93–101 (2006).
11. J. M. Spergel, T. Brown-Whitehorn, The use of patch testing in the diagnosis of food allergy. *Curr. Allergy Asthma Rep.* **5**, 86–90 (2005).
12. R. Spiewak, Patch testing for contact allergy and allergic contact dermatitis. *Open Allergy J.* **1**, 42–51 (2008).
13. D. Tatovic, P. Young, E. Kochba, Y. Levin, F. S. Wong, C. M. Dayan, Fine-needle aspiration biopsy of the lymph node: A novel tool for the monitoring of immune responses after skin antigen delivery. *J. Immunol.* **195**, 386–392 (2015).
14. J. R. Bjerke, J. K. Livden, M. Degré, R. Matre, Interferon in suction blister fluid from psoriatic lesions. *Br. J. Dermatol.* **108**, 295–299 (1983).
15. M. R. Prausnitz, Engineering microneedle patches for vaccination and drug delivery to skin. *Annu. Rev. Chem. Biomol. Eng.* **8**, 177–200 (2017).
16. P. M. Wang, M. Cornwell, M. R. Prausnitz, Minimally invasive extraction of dermal interstitial fluid for glucose monitoring using microneedles. *Diabetes Technol. Ther.* **7**, 131–141 (2005).
17. A. C. I. Depelsenaire, S. C. Meliga, C. L. Mcneilly, F. E. Pearson, J. W. Coffey, O. L. Haigh, C. J. Flaim, I. H. Frazer, M. A. F. Kendall, Colocalization of cell death with antigen deposition in skin enhances vaccine immunogenicity. *J. Invest. Dermatol.* **134**, 2361–2370 (2014).
18. P. C. DeMuth, W. F. Garcia-Beltran, M. L. Ai-Ling, P. T. Hammond, D. J. Irvine, Composite dissolving microneedles for coordinated control of antigen and adjuvant delivery kinetics in transcutaneous vaccination. *Adv. Funct. Mater.* **23**, 161–172 (2013).
19. J. Hong, N. J. Shah, A. C. Drake, P. C. DeMuth, J. B. Lee, J. Chen, P. T. Hammond, Graphene multilayers as gates for multi-week sequential release of proteins from surfaces. *ACS Nano* **6**, 81–88 (2012).
20. J. J. Moon, H. Suh, A. Bershteyn, M. T. Stephan, H. Liu, B. Huang, M. Sohail, S. Luo, S. H. Um, H. Khant, J. T. Goodwin, J. Ramos, W. Chiu, D. J. Irvine, Interbilayer-crosslinked multilamellar vesicles as synthetic vaccines for potent humoral and cellular immune responses. *Nat. Mater.* **10**, 243–251 (2011).
21. J. Kool, L. Reubsaet, F. Wesseldijk, R. T. Maravilha, M. W. Pinkse, C. S. D'Santos, J. J. van Hilten, F. J. Zijlstra, A. J. R. Heck, Suction blister fluid as potential body fluid for biomarker proteins. *Proteomics* **7**, 3638–3650 (2007).
22. M. P. Hedger, S. Herriarachchi, Measurement of immunoglobulin G levels in adult rat testicular interstitial fluid and serum. *J. Androl.* **15**, 583–590 (1994).
23. W. C. Weldon, V. G. Zarnitsyn, E. S. Esser, M. T. Taherbhai, D. G. Koutsonanos, E. V. Vassilieva, I. Skountzou, M. R. Prausnitz, R. W. Compans, M. M. Rodrigues, Effect of adjuvants on responses to skin immunization by microneedles coated with influenza subunit vaccine. *PLOS ONE* **7**, e41501 (2012).
24. Y. Lai, A. Di Nardo, T. Nakatsuji, A. Leichtle, Y. Yang, A. L. Cogen, Z.-R. Wu, L. V. Hooper, R. R. Schmidt, S. von Aulock, K. A. Radek, C.-M. Huang, A. F. Ryan, R. L. Gallo, Commensal bacteria regulate toll-like receptor 3–dependent inflammation after skin injury. *Nat. Med.* **15**, 1377–1382 (2009).
25. W. Weninger, M. Biro, R. Jain, Leukocyte migration in the interstitial space of non-lymphoid organs. *Nat. Rev. Immunol.* **14**, 232–246 (2014).
26. P. Guermonprez, L. Saveanu, M. Kleijmeer, J. Davoust, P. van Endert, S. Amigorena, ER–phagosome fusion defines an MHC class I cross-presentation compartment in dendritic cells. *Nature* **425**, 397–402 (2003).
27. J. M. Schenkel, K. A. Fraser, L. K. Beura, K. E. Pauken, D. Masopust, V. Vezys, D. Masopust, Resident memory CD8 T cells trigger protective innate and adaptive immune responses. *Science* **346**, 98–101 (2014).

28. L. Liu, R. C. Fuhlbrigge, K. Karibian, T. Tian, T. S. Kupper, Dynamic programing of $CD8^+$ T cell trafficking after live viral immunization. *Immunity* **25**, 511–520 (2006).
29. J. W. Coffey, S. R. Corrie, M. A. F. Kendall, Early circulating biomarker detection using a wearable microprojection array skin patch. *Biomaterials* **34**, 9572–9583 (2013).
30. S. P. Sullivan, D. G. Koutsonanos, M. Del Pilar Martin, J. W. Lee, V. Zarnitsyn, S.-O. Choi, N. Murthy, R. W. Compans, I. Skountzou, M. R. Prausnitz, Dissolving polymer microneedle patches for influenza vaccination. *Nat. Med.* **16**, 915–920 (2010).
31. M. Zaric, O. Lyubomska, C. Poux, M. L. Hanna, M. T. McCrudden, B. Malissen, R. J. Ingram, U. F. Power, C. J. Scott, R. F. Donnelly, A. Kissenpfennig, Dissolving microneedle delivery of nanoparticle-encapsulated antigen elicits efficient cross-priming and Th1 immune responses by murine langerhans cells. *J. Invest. Dermatol.* **135**, 425–434 (2015).
32. A. Mildner, S. Jung, Development and function of dendritic dell subsets. *Immunity* **40**, 642–656 (2014).
33. K. Mooney, J. C. McElnay, R. F. Donnelly, Children's views on microneedle use as an alternative to blood sampling for patient monitoring. *Int. J. Pharm. Pract.* **22**, 335–344 (2014).
34. C. G. Lian, E. M. Bueno, S. R. Granter, A. C. Laga, A. P. Saavedra, W. M. Lin, J. S. Susa, Q. Zhan, A. K. Chandraker, S. G. Tullius, B. Pomahac, G. F. Murphy, Biomarker evaluation of face transplant rejection: Association of donor T cells with target cell injury. *Mod. Pathol.* **27**, 788–799 (2014).
35. Y. Ma, W. Tao, S. J. Krebs, W. F. Sutton, N. L. Haigwood, H. S. Gill, Vaccine delivery to the oral cavity using coated microneedles induces systemic and mucosal immunity. *Pharm. Res.* **31**, 2393–2403 (2014).
36. N. Wang, Y. Zhen, Y. Jin, X. Wang, N. Li, S. Jiang, T. Wang, Combining different types of multifunctional liposomes loaded with ammonium bicarbonate to fabricate microneedle arrays as a vaginal mucosal vaccine adjuvant-dual delivery system (VADDS). *J. Control. Release* **246**, 12–29 (2017).
37. Q. Zeng, J. M. Gammon, L. H. Tostanoski, Y.-C. Chiu, C. M. Jewell, In vivo expansion of melanoma-specific T cells using microneedle arrays coated with immune-polyelectrolyte multilayers. *ACS Biomater Sci. Eng.* **3**, 195–205 (2017).
38. P. C. Demuth, J. J. Moon, H. Suh, P. T. Hammond, D. J. Irvine, Releasable layer-by-layer assembly of stabilized lipid nanocapsules on microneedles for enhanced transcutaneous vaccine delivery. *ACS Nano* **6**, 8041–8051 (2012).
39. H. Liu, K. D. Moynihan, Y. Zheng, G. L. Szeto, A. V. Li, B. Huang, D. S. Van Egeren, C. Park, D. J. Irvine, Structure-based programming of lymph-node targeting in molecular vaccines. *Nature* **507**, 519–522 (2014).

Acknowledgments: We thank K. Rakhra, T. Tokatlian, E. L. Dane, T. Gierahn, M. B. Melo, and H. Watkins for technical expertise and advice. **Funding:** This work was supported in part by the Ragon Institute of MGH, MIT and Harvard, the Koch Institute Support (core) Grant P30-CA14051 from the National Cancer Institute, and the U. S. Army Research Laboratory and the U. S. Army Research Office through the Institute for Soldier Nanotechnologies under contract number W911NF-13-D-0001. D.J.I. is an investigator of the Howard Hughes Medical Institute. **Author contributions:** A.M., A.V.B., P.T.H., and D.J.I. designed the experiments and analyzed the data. A.M. and A.V.B. carried out the material characterization. A.M. synthesized SSMNs and carried out the in vivo experiments. A.M., D.J.I., P.T.H., and J.C.L. wrote the manuscript. L.K.W.L. designed and performed the imaging cytometry experiments. K.D.M. prepared the material for OVA and lipo-CpG vaccinations. M.E.W. designed and performed the atomic force microscopy experiments. N.R.B. provided the technical support for fluorophore labeling of alginate. N.R.B. and N.T. performed the protein quantification accuracy and polyI:C stability experiments. M.E.T. performed the human skin sampling microneedle experiments. J.H.V. provided the technical support for SSMN preparation and in vivo studies. **Competing interests:** The authors declare that they have no competing interests. **Data and materials availability:** All data associated with this study are present in the paper or the Supplementary Materials.

Submitted 16 October 2017
Resubmitted 24 April 2018
Accepted 15 October 2018
Published 14 November 2018
10.1126/scitranslmed.aar2227

Citation: A. Mandal, A. V. Boopathy, L. K. W. Lam, K. D. Moynihan, M. E. Welch, N. R. Bennett, M. E. Turvey, N. Thai, J. H. Van, J. C. Love, P. T. Hammond, D. J. Irvine, Cell and fluid sampling microneedle patches for monitoring skin-resident immunity. *Sci. Transl. Med.* **10**, eaar2227 (2018).

Science Translational Medicine

Cell and fluid sampling microneedle patches for monitoring skin-resident immunity

Anasuya Mandal, Archana V. Boopathy, Lionel K. W. Lam, Kelly D. Moynihan, Mary E. Welch, Nitasha R. Bennett, Michelle E. Turvey, Nikki Thai, Jenny H. Van, J. Christopher Love, Paula T. Hammond and Darrell J. Irvine

Sci Transl Med **10**, eaar2227.
DOI: 10.1126/scitranslmed.aar2227

Tissues are the window into the immune system

Immune status and responses are often determined by analyzing circulating cells isolated from the blood. However, many immune processes and diseases depend on tissue-resident immune cells acting in target organs, which would not be reflected in peripheral immune cells. To sample these tissue-resident cells, Mandal *et al*. designed a microneedle array that can be applied to the skin. These microneedles can be loaded with adjuvants and antigens of interest to draw in responding immune cells. The microneedles are noninvasive and can be used to follow immune responses over time; similar sampling could be done in the future for other tissues. Tools such as these microneedles can help scientists gain a more accurate understanding of immune responses.